Incremental Deadbeat Predictive Current Control Strategy With Disturbance Observer for PMSM Drive Systems Using Four-Leg Inverters

Yuchen Zhou, Liang Yan, *Senior Member, IEEE*, Xiaocheng Wei, and Mostafa S. Hamad, *Senior Member, IEEE*

***Abstract*—Deadbeat predictive current control (DPCC) has been implemented in four-leg inverters to obtain faster dynamic response and higher system bandwidth, and effectively reduce the machine torque ripple caused by current tracking error after open-phase fault. However, DPCC is a kind of model-parameter-sensitive control method, so inaccurate model parameters may cause deviations in the current prediction and reduce control performance. To address this issue, an incremental deadbeat predictive current control strategy with sliding mode disturbance observer (IDPCC+SMDO) is proposed in this article. Detailed studies are carried out to validate the parameter robustness of the proposed method. Initially, the permanent magnet synchronous motor model with connected neutral point is conducted, followed by the parameter sensitivity analysis of conventional DPCC method. Subsequently, an incremental prediction model is established to eliminate the effects of permanent magnet flux linkage mismatch on the prediction results. Furthermore, a sliding mode observer is designed for the compensation of disturbances and uncertainties caused by inductance and resistance mismatches. Finally, the effectiveness of the proposed IDPCC + SMDO method is verified by comprehensive simulations and experiments. The results demonstrate that the proposed method can suppress the negative impact of parameter mismatches on the control performance in both healthy and open-phase fault-tolerant operation modes.**

Received 12 December 2024; revised 10 March 2025, 29 April 2025, and 10 June 2025; accepted 10 July 2025. Date of publication 15 July 2025; date of current version 27 August 2025. This work was supported in part by the National Key Research and Development Program under Grant 2022YFE0113700, in part by the National Natural Science Foundation of China (NSFC) under Grant 52130505, in part by the Zhejiang Provincial Natural Science Foundation of China under Grant LD24E050005, in part by the Ningbo Key Scientific and Technological Project under Grant 2022Z040, and in part by the Fundamental Research Funds for the Central Universities. Recommended for publication by Associate Editor A. M. Bazzi. *(Corresponding author: Liang Yan.)*

Yuchen Zhou is with the School of Automation Science and Electrical Engineering, Beihang University, Beijing 100191, China (e-mail: asherzhou@buaa.edu.cn).

Liang Yan is with the School of Automation Science and Electrical Engineering, Beihang University, Beijing 100191, China, also with the Ningbo Institute of Technology, Beihang University, Ningbo 315800, China, also with Tianmushan Laboratory, Hangzhou 310023, China, and also with Science and Technology on Aircraft Control Laboratory, Beihang University, Beijing 10091, China (e-mail: yanliang@buaa.edu.cn).

Xiaocheng Wei is with the Ningbo Institute of Technology, Beihang University, Ningbo 315800, China (e-mail: xiaocheng.wei@buaa.edu.cn).

Mostafa S. Hamad is with the Research and Innovation Center, Arab Academy for Science, Technology and Maritime Transport, Alamein 51718, Egypt (e-mail: mostafa.hamad@staff.aast.edu).

Color versions of one or more figures in this article are available at https://doi.org/10.1109/TPEL.2025.3589453.

Digital Object Identifier 10.1109/TPEL.2025.3589453

***Index Terms*—Deadbeat predictive current control (DPCC), disturbance observer, fault-tolerant control, four-leg inverter, permanent magnet synchronous motor (PMSM).**

I. Introduction

THE reliability and robustness of permanent magnet synchronous motor (PMSM) drive systems have always been a hotspot of academic research in power transmission applications that require uninterrupted operation during a single task cycle, such as the driving system of electric vehicles [1], [2], the actuation system of more electric aircraft [3], and the motion system of industrial robot [4]. According to statistics, the open-phase fault is one of the main failure types in motor drive systems, caused by the open circuit of windings or power semiconductor devices, and may result in the loss of current control in a certain phase [5]. In addition, the short circuit of power semiconductor devices, the loss of gate control signals, and the disconnection of cables between PMSMs and inverters can also be converted into open-phase fault for processing [6], [7]. Therefore, it is significant to study the fault-tolerant control strategy of PMSM drive systems after phase loss.

Increasing the number of winding phases is a mainstream method to strengthen the open-phase fault-tolerant capability of PMSM drive systems, such as using five-phase windings, dual-three-phase windings, and nine-phase windings. [8], [9], [10]. After an open-phase fault occurs, the multiphase PMSM drive systems can continue to operate by isolating the faulty phases and using the remaining healthy phases to reconstruct a stable circular rotating stator magnetic field. However, the high manufacturing cost of multiphase PMSM drive systems and the complicated control strategy make their narrower application range. Moreover, three-phase motors are still the main equipment in current industrial applications. Hence, it is significant and meaningful to develop the open-phase fault-tolerant control strategy for three-phase PMSM drive systems.

By connecting the neutral point of the three-phase PMSM's star-connected winding to the redundant leg of four-leg inverter, the neutral line current can be controlled to compensate for the negative-sequence magnetomotive force component after open-phase fault, and then the three-phase motor has fault-tolerant operation capability [11]. When the PMSM switches from the

healthy operation mode to fault-tolerant operation mode, only the zero-axis current reference needs to be reconfigured, and the control strategy and machine model can be kept constant to avoid attached uncertainties and unnecessary disturbances [6]. However, the zero-axis current reference is a rotor-position-dependent sinusoidal waveform, which presents a challenge for the proportional–integral (PI) controller to achieve zero-error tracking, as it is inherently a linear controller [12]. To address this issue, scholars have developed some current predictive control methods for four-leg inverters, such as finite-control-set model predictive current control (FCS-MPCC) [13], continuous-control-set model predictive current control (CCS-MPCC) [14], and deadbeat predictive current control (DPCC) [15]. Compared with FCS-MPCC, DPCC has better steady-state current tracking performance by introducing the pulse width modulator. Meanwhile, since DPCC does not require the complex multistep prediction and optimization processes, the computation burden of DPCC is less than that of MPCC [16]. These characteristics make DPCC have great application potential in the field of high-performance PMSM drive systems [15].

However, DPCC is a kind of model-parameter-sensitive control method, so inaccurate model parameters may cause deviations in the current prediction results and increase torque ripple. Meanwhile, the accuracy of PMSM current prediction model is affected by temperature changes, magnetic saturation, cross-coupling, and other factors [17], [18]. In order to solve this problem, researchers mainly improved the robustness of DPCC algorithm by online parameter identification and disturbance observers. Online parameter identification methods can estimate the values of PMSM parameters during operation, mainly including the recursive least-squares [19], [20], the model reference-based adaptive system [21], and the extended Kalman filter [22], etc. The PMSM model parameters used for current prediction can be dynamically updated with estimated motor parameter values, thereby improving the parameter robustness of DPCC. However, these online parameter identification algorithms are complex and require high-performance processors [23]. In addition, several online parameter identification methods using high-frequency current injection may increase the copper loss and reduce the efficiency of PMSM drive systems [24].

Another mainstream approach to compensate for prediction errors caused by parameter mismatches and unknown interferences is to introduce disturbance observers. A Luenberger disturbance observer proposed in [25] is to estimate the lumped disturbances in the speed and current loop. In [26], the sampled currents in the prediction model are replaced by the estimated currents calculated by an extended state observer to address the disturbances caused by parameter mismatches and one-step delay. Compared to other disturbance observers, the sliding mode disturbance observer (SMDO) is regarded as having superior robustness against all types of system disturbances, making it a hotspot both in academia and industry [27]. A composite control method combining DPCC and SMDO is developed in [28] to simultaneously predict stator current and compensate system disturbances caused by parameter mismatches. The outputs of SMDO are used as the feedforward values to compensate the voltage reference calculated by deadbeat predictive current controller. Similar methods are also reported in [29] and [30]. However, these methods have only been analyzed and applied in PMSM drive systems using three-leg inverters instead of four-leg inverters. Hence, the performance of DPCC in PMSM drive systems using four-leg inverters needs to be further evaluated, especially in the fault-tolerant operation mode.

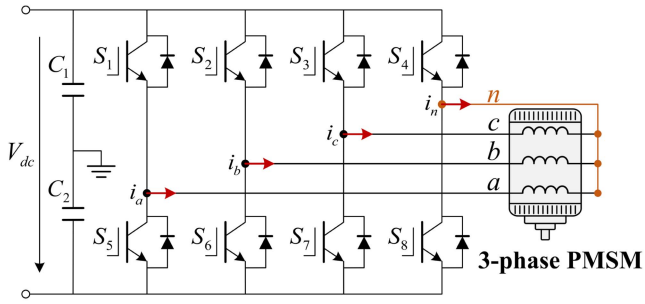

Fig. 1. Three-phase PMSM fault-tolerant drive topology using a four-leg inverter.

Therefore, the objective of this article is to propose an incremental deadbeat predictive current control strategy with sliding mode disturbance observer (IDPCC + SMDO) for PMSM drive systems using four-leg inverters, aimed at enhancing the fault-tolerant performance and parameter robustness. In this approach, an incremental prediction model is employed to eliminate the impact of permanent magnet flux linkage mismatch on the prediction results. A disturbance observer based on sliding-mode exponential reaching law is designed for the compensation of disturbances caused by resistance and inductance mismatches in the incremental prediction model. Since the current prediction error caused by parameter mismatches is suppressed by the incremental model and SMDO, the proposed IDPCC + SMDO method ensures satisfactory steady-state and dynamic performance in both healthy and fault-tolerant operation modes.

The rest of this article is organized as follows. In Section II, the mathematical model of PMSM with connected neutral point and DPCC method are introduced, and the parameter sensitivity analysis is conducted to illustrate the impact of parameter mismatches on current prediction results. Section III presents the proposed IDPCC + SMDO method. In Section IV, the performance comparison between conventional DPCC and the proposed IDPCC + SMDO method under parameter mismatches is conducted by simulation. In Section V, one research prototype along with the test rig has been developed, and experimental tests are conducted to verify the effectiveness of proposed IDPCC + SMDO method. Finally, Section VI concludes this aticle.

II. PMSM Mathematical Model and Conventional DPCC Method Analysis

A. Model of the PMSM With Connected Neutral Point

The fault-tolerant drive topology of three-phase PMSM using a four-leg inverter is shown in Fig. 1. The neutral point of the PMSM's star-connected winding is permanently connected to the fourth leg of inverter. The motor discussed in this article

is a surface-mounted PMSM, which means that the effect of saliency can be neglected. When magnetic saturation is ignored, the voltage equations of machine can be expressed in the $dq0$ synchronous reference frame as

$$\begin{bmatrix} u_d \\ u_q \\ u_0 \end{bmatrix} = R_s \begin{bmatrix} i_d \\ i_q \\ i_0 \end{bmatrix} + \begin{bmatrix} L_{dq} & 0 & 0 \\ 0 & L_{dq} & 0 \\ 0 & 0 & L_0 \end{bmatrix} \frac{\mathrm{d}}{\mathrm{d}t} \begin{bmatrix} i_d \\ i_q \\ i_0 \end{bmatrix} + \omega_e \begin{bmatrix} -L_{dq} i_q \\ L_{dq} i_d + \psi_\mathrm{f} \\ 0 \end{bmatrix} \tag{1}$$

where u_y and i_y ($y \in \{d, q, 0\}$) are the voltage and current of y-axis component in the synchronous rotating reference frame, respectively. R_s, ψ_f, and ω_e represent the stator resistance, the permanent magnet flux linkage, and the electrical angular velocity of the rotor, respectively. L_{dq} and L_0 are the dq-axis inductance and zero-axis inductance, respectively.

When the PMSM is in healthy operation mode, the three-phase current is sinusoidal and the phase difference between them is 120°, so the zero-axis current i_0 is zero. In order not to affect the machine output torque, the zero-axis current i_0 should be redistributed to keep i_d and i_q unchanged when the open-phase fault occurs [6]. If an open-circuit fault occurs on phase A, then i_0 should be adjusted to

$$i_0^{af} = \sqrt{2}\left[i_q \sin(\theta_e) - i_d \cos(\theta_e)\right] \tag{2}$$

where θ_e is the rotor electrical position. Similarly, when the open-phase fault occurs in phase B and phase C, the zero-axis current component i_0 should be adjusted to

$$i_0^{bf} = \sqrt{2}\left[i_q \sin(\theta_e - 2\pi/3) - i_d \cos(\theta_e - 2\pi/3)\right] \tag{3}$$

and

$$i_0^{cf} = \sqrt{2}\left[i_q \sin(\theta_e + 2\pi/3) - i_d \cos(\theta_e + 2\pi/3)\right] \tag{4}$$

respectively. It can be seen from (2)–(4) that i_0 should be changed into an ac component that varies with rotor position to maintain the dq-axis currents unchanged when the PMSM is in fault-tolerant operation mode. However, it is difficult for PI controllers to achieve zero-error tracking of ac components.

B. Conventional DPCC

In order to design the predictive current digital controller, the forward first-order Euler discretization is applied to (1) to obtain the predictive currents at the $(k+1)$th instant

$$\begin{bmatrix} i_d(k+1) \\ i_q(k+1) \\ i_0(k+1) \end{bmatrix} = A(k) \begin{bmatrix} i_d(k) \\ i_q(k) \\ i_0(k) \end{bmatrix} + B \begin{bmatrix} u_d(k) \\ u_q(k) \\ u_0(k) \end{bmatrix} + E(k) \tag{5}$$

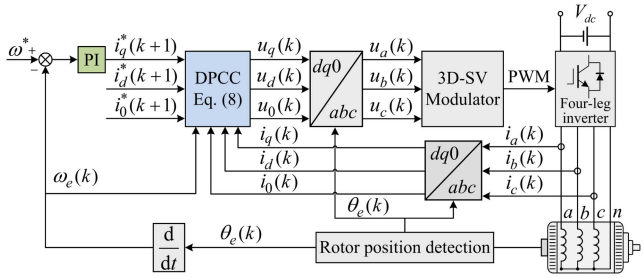

Fig. 2. Block diagram of DPCC for PMSMs using four-leg inverters.

$$A(k) = \begin{bmatrix} 1 - \frac{T_c R_s}{L_{dq}} & T_c \omega_e(k) & 0 \\ -T_c \omega_e(k) & 1 - \frac{T_c R_s}{L_{dq}} & 0 \\ 0 & 0 & 1 - \frac{T_c R_s}{L_0} \end{bmatrix}$$

$$B = \begin{bmatrix} \frac{T_c}{L_{dq}} & 0 & 0 \\ 0 & \frac{T_c}{L_{dq}} & 0 \\ 0 & 0 & \frac{T_c}{L_0} \end{bmatrix}, \quad E(k) = \begin{bmatrix} 0 \\ -\frac{T_c \psi_\mathrm{f}}{L_{dq}} \omega_e(k) \\ 0 \end{bmatrix} \tag{6}$$

where $u_d(k)$, $u_q(k)$, and $u_0(k)$ are the $dq0$-axis stator voltages at the kth instant, respectively. $i_y(k)$ and $i_y(k+1)$ ($y \in \{d, q, 0\}$) are the stator currents in the synchronous rotating frame at the kth and $(k+1)$th instant, respectively. $\omega_e(k)$ is the electrical angular velocity at the kth instant. T_c denotes the execution period of the digital control system and the phase current sampling time. From (5), the output control voltages of the DPCC method at the kth instant is

$$\begin{bmatrix} u_d(k) \\ u_q(k) \\ u_0(k) \end{bmatrix} = B^{-1} \left(\begin{bmatrix} i_d(k+1) \\ i_q(k+1) \\ i_0(k+1) \end{bmatrix} - A(k) \begin{bmatrix} i_d(k) \\ i_q(k) \\ i_0(k) \end{bmatrix} - E(k) \right). \tag{7}$$

In order to make the actual currents generated by the output control voltages of DPCC method approach the reference currents at the next instant, the $(k+1)$th instant currents $i_d(k+1)$, $i_q(k+1)$, and $i_0(k+1)$ should be replaced by reference currents $i_d^*(k+1)$, $i_q^*(k+1)$, and $i_0^*(k+1)$. Therefore, the output control voltages can be expressed as

$$\begin{bmatrix} u_d(k) \\ u_q(k) \\ u_0(k) \end{bmatrix} = B^{-1} \left(\begin{bmatrix} i_d^*(k+1) \\ i_q^*(k+1) \\ i_0^*(k+1) \end{bmatrix} - A(k) \begin{bmatrix} i_d(k) \\ i_q(k) \\ i_0(k) \end{bmatrix} - E(k) \right). \tag{8}$$

The structure of DPCC for PMSM drive systems using four-leg inverters is shown in Fig. 2. The q-axis current reference is the output of speed loop PI controller. The motor speed is adjusted by modulating the PMSM output torque to achieve the target speed ω^*, which necessitates precise tracking of the reference by the q-axis current i_q. The d-axis current i_d is typically employed for flux-weakening control, with its reference set to zero in surface-mounted PMSMs to maximize efficiency by minimizing copper

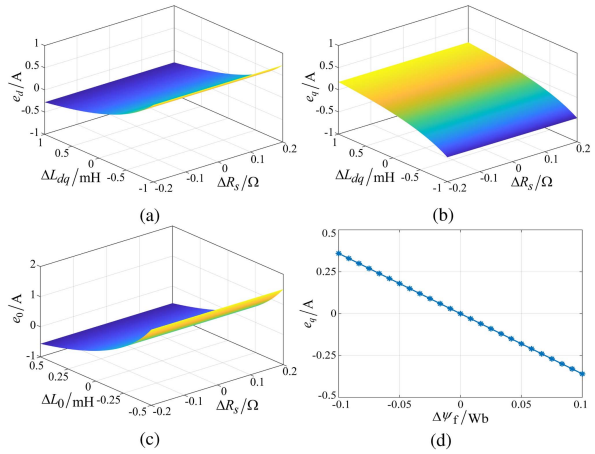

Fig. 3. Relationship between the prediction error of $dq0$-axis currents and the machine parameter mismatches. (a) d-axis current prediction error under dq-axis inductance and resistance mismatches. (b) q-axis current prediction error under dq-axis inductance and resistance mismatches. (c) Zero-axis current prediction error under zero-axis inductance and resistance mismatches. (d) q-axis current prediction error under permanent magnet flux linkage mismatch.

losses. When the machine is in healthy operation mode, the reference of i_0 is set to zero. When an open circuit fault occurs, the reference of i_0 should be adjusted to (2)–(4) according to the phase fault location. Based on the sampled currents at the kth instant and the reference currents at the $(k+1)$th instant, the output control voltages of DPCC method can be calculated by (8). Then, the control voltages are applied to the motor windings by the four-leg inverter through the 3-D space vector modulator in natural abc reference frame [31], [32].

C. Parameter Sensitivity Analysis

As depicted by (8), the prediction results of DPCC are affected by motor parameters, including the stator resistance R_s, dq-axis inductance L_{dq}, zero-axis inductance L_0, and permanent magnet flux linkage ψ_{f}. Hence, the accuracy of machine parameters used in prediction model may directly influence the control performance in the PMSM drive system. Therefore, the parameter sensitivity analysis is conducted in this section to illustrate the impact of parameter mismatches on current prediction results of DPCC method.

From (5), the predictive currents of DPCC method under motor parameter mismatches can be expressed as follows:

$$\begin{bmatrix} i'_d(k+1) \\ i'_q(k+1) \\ i'_0(k+1) \end{bmatrix} = A'(k) \begin{bmatrix} i_d(k) \\ i_q(k) \\ i_0(k) \end{bmatrix} + B' \begin{bmatrix} u_d(k) \\ u_q(k) \\ u_0(k) \end{bmatrix} + E'(k) \quad (9)$$

$$A'(k) = \begin{bmatrix} 1-\frac{T_c(R_s+\Delta R_s)}{L_{dq}+\Delta L_{dq}} & T_c\omega_e(k) & 0 \\ -T_c\omega_e(k) & 1-\frac{T_c(R_s+\Delta R_s)}{L_{dq}+\Delta L_{dq}} & 0 \\ 0 & 0 & 1-\frac{T_c(R_s+\Delta R_s)}{L_0+\Delta L_0} \end{bmatrix}$$

$$B' = \mathrm{diag}\left[\frac{T_c}{L_{dq}+\Delta L_{dq}} \quad \frac{T_c}{L_{dq}+\Delta L_{dq}} \quad \frac{T_c}{L_0+\Delta L_0}\right]$$

TABLE I
TESTED PMSM PARAMETERS

Parameters	Symbol	Value	Unit
Number of pole pairs	p	4	– –
Rated power	P_N	2.3	kW
Rated speed	N	1500	r/min
Stator resistance	R_s	0.55	Ω
dq-axis inductance	L_{dq}	2.225	mH
Zero-axis inductance	L_0	1.1	mH
Permanent magnet flux linkage	ψ_{f}	0.218	Wb

$$E'(k) = \begin{bmatrix} 0 & -\frac{T_c(\psi_{\mathrm{f}}+\Delta\psi_{\mathrm{f}})}{L_{dq}+\Delta L_{dq}}\omega_e(k) & 0 \end{bmatrix}^T \quad (10)$$

where ΔR_s, ΔL_{dq}, ΔL_0, and $\Delta\psi_{\mathrm{f}}$ are the difference between the parameter values of stator resistance, dq-axis inductance, zero-axis inductance, and permanent magnet flux linkage used for predictive currents calculation and the actual machine parameter values. Therefore, the prediction errors of DPCC method caused by parameter mismatches can be expressed as follows:

$$e_y = i'_y(k+1) - i_y(k+1), y \in \{d, q, 0\} \quad (11)$$

with

$$\begin{cases} e_d = \frac{R_s\Delta L_{dq}-L_{dq}\Delta R_s}{L_{dq}(L_{dq}+\Delta L_{dq})}T_c i_d(k) - \frac{\Delta L_{dq}}{L_{dq}(L_{dq}+\Delta L_{dq})}T_c u_d(k) \\ e_q = \frac{R_s\Delta L_{dq}-L_{dq}\Delta R_s}{L_{dq}(L_{dq}+\Delta L_{dq})}T_c i_q(k) - \frac{\Delta L_{dq}}{L_{dq}(L_{dq}+\Delta L_{dq})}T_c u_q(k) \\ \qquad + \frac{\psi_{\mathrm{f}}\Delta L_{dq}-L_{dq}\Delta\psi_{\mathrm{f}}}{L_{dq}(L_{dq}+\Delta L_{dq})}T_c\omega_e(k) \\ e_0 = \frac{R_s\Delta L_0-L_0\Delta R_s}{L_0(L_0+\Delta L_0)}T_c i_0(k) - \frac{\Delta L_0}{L_0(L_0+\Delta L_0)}T_c u_0(k). \end{cases} \quad (12)$$

It can be observed from (12) that the $dq0$-axis predictive currents are all influenced by the stator resistance error ΔR_s, while the d- and zero-axes currents remain unaffected by the permanent magnet flux linkage error $\Delta\psi_{\mathrm{f}}$. In addition, the dq-axis inductance error ΔL_{dq} impacts both the d-axis and q-axis predictive currents, whereas the zero-axis inductance error ΔL_0 only affects the zero-axis current. Furthermore, the current prediction errors are all dependent on mechanical parameters, motor speed, and sampled currents.

Fig. 3 shows the relationship between the $dq0$-axis current prediction errors and the mismatches in stator resistance, dq-axis inductance, zero-axis inductance, and permanent magnet flux linkage. The parameters of tested PMSM are listed in Table I and the speed is set to 1200 r/min. As shown in Fig. 3(a)–(c), the stator resistance error ΔR_s has minimal effect on the $dq0$-axis predictive currents when the inductance mismatch remains unchanged. In contrast, the inductance errors ΔL_{dq} and ΔL_0 significantly influence current prediction, exhibiting a nonlinear relationship with the prediction errors. Therefore, when the inductance values used in the prediction model differ from the actual values, compensating for the prediction error with a constant becomes challenging. As depicted in Fig. 3(d), the q-axis current prediction error is proportional to the permanent magnet

flux linkage error $\Delta\psi_{\mathrm{f}}$, indicating that the error of flux linkage may introduce a constant offset between the q-axis reference current and the actual current.

In addition, there is a one-step delay between current sampling and output control voltage loading because the microprocessor executes instructions serially, which may deteriorate the performance of PMSM drive system [33], [34]. Therefore, an incremental DPCC strategy with sliding mode disturbance observer (IDPCC + SMDO) is proposed in Section III to mitigate the current tracking performance degradation caused by parameter mismatches and one-step delay, thereby ensuring satisfactory control performance in both healthy and fault-tolerant operation modes.

III. Proposed IDPCC + SMDO Method

A. Establishment of Incremental Prediction Model

According to the abovementioned parameter sensitivity analysis of DPCC method, the permanent magnet flux linkage mismatch can cause q-axis current prediction error, thus exerting a substantial influence on the motor torque control. Therefore, an incremental prediction model is created in this section to eliminate the effect of flux linkage mismatch. According to (7), the voltages at the $(k-1)$th instant can be expressed as follows:

$$\begin{bmatrix} u_d(k-1) \\ u_q(k-1) \\ u_0(k-1) \end{bmatrix} = B^{-1}\left(\begin{bmatrix} i_d(k) \\ i_q(k) \\ i_0(k) \end{bmatrix} - A(k-1) \begin{bmatrix} i_d(k-1) \\ i_q(k-1) \\ i_0(k-1) \end{bmatrix} - E(k-1) \right). \tag{13}$$

Since the mechanical dynamics of motors are much slower than the electrical dynamics, the electrical angular velocity can be considered constant during successive sampling periods, i.e., $\omega_e(k) = \omega_e(k-1)$. Hence, $A(k) = A(k-1)$ and $E(k) = E(k-1)$. Subtracting (13) from (7), the incremental voltages at the kth instant relative to the $(k-1)$th instant is

$$\begin{bmatrix} u_d(k) \\ u_q(k) \\ u_0(k) \end{bmatrix} = \begin{bmatrix} u_d(k-1) \\ u_q(k-1) \\ u_0(k-1) \end{bmatrix} + B^{-1}\left(\begin{bmatrix} \Delta i_d(k+1) \\ \Delta i_q(k+1) \\ \Delta i_0(k+1) \end{bmatrix} - A(k) \begin{bmatrix} \Delta i_d(k) \\ \Delta i_q(k) \\ \Delta i_0(k) \end{bmatrix} \right) \tag{14}$$

where

$$\begin{cases} \Delta i_y(k) = i_y(k) - i_y(k-1) \\ \Delta i_y(k+1) = i_y(k+1) - i_y(k) \end{cases}, y \in \{d, q, 0\}. \tag{15}$$

In order to make the actual currents generated by the output voltages of controller approach the reference currents at the next instant, the $(k+1)$th instant currents $i_d(k+1)$, $i_q(k+1)$, and $i_0(k+1)$ should be replaced by reference currents $i_d^*(k+1)$, $i_q^*(k+1)$, and $i_0^*(k+1)$, respectively.

As observed from (14) and (15), the incremental prediction model of PMSM with connected neutral point can eliminate the effect of flux linkage mismatch on current prediction. However, the presence of resistance and inductance remains within the incremental prediction model, so the impact of resistance and inductance mismatches must be considered.

B. Sliding Mode Disturbance Observer Design

According to (1), the voltage equation of PMSM with connected neutral point considering parameter mismatches is

$$\begin{bmatrix} u_d \\ u_q \\ u_0 \end{bmatrix} = R_s \begin{bmatrix} i_d \\ i_q \\ i_0 \end{bmatrix} + \begin{bmatrix} L_{dq} & 0 & 0 \\ 0 & L_{dq} & 0 \\ 0 & 0 & L_0 \end{bmatrix} \frac{\mathrm{d}}{\mathrm{d}t} \begin{bmatrix} i_d \\ i_q \\ i_0 \end{bmatrix} + \omega_e \begin{bmatrix} -L_{dq} i_q \\ L_{dq} i_d + \psi_{\mathrm{f}} \\ 0 \end{bmatrix} + \begin{bmatrix} f_d \\ f_q \\ f_0 \end{bmatrix} \tag{16}$$

where f_d, f_q, and f_0 are the parameter disturbances caused by the variation of stator resistance, dq-axis inductance, zero-axis inductance, and permanent magnet flux linkage. Therefore, the parameter disturbances can be expressed as follows:

$$\begin{bmatrix} f_d \\ f_q \\ f_0 \end{bmatrix} = \Delta R_s \begin{bmatrix} i_d \\ i_q \\ i_0 \end{bmatrix} + \begin{bmatrix} \Delta L_{dq} & 0 & 0 \\ 0 & \Delta L_{dq} & 0 \\ 0 & 0 & \Delta L_0 \end{bmatrix} \frac{\mathrm{d}}{\mathrm{d}t} \begin{bmatrix} i_d \\ i_q \\ i_0 \end{bmatrix} + \omega_e \begin{bmatrix} -\Delta L_{dq} i_q \\ \Delta L_{dq} i_d + \Delta\psi_{\mathrm{f}} \\ 0 \end{bmatrix}. \tag{17}$$

In order to estimate the above parameter disturbances, the disturbance observer can be designed as follows:

$$\begin{bmatrix} u_d \\ u_q \\ u_0 \end{bmatrix} = R_s \begin{bmatrix} \hat{i}_d \\ \hat{i}_q \\ \hat{i}_0 \end{bmatrix} + \begin{bmatrix} L_{dq} & 0 & 0 \\ 0 & L_{dq} & 0 \\ 0 & 0 & L_0 \end{bmatrix} \frac{\mathrm{d}}{\mathrm{d}t} \begin{bmatrix} \hat{i}_d \\ \hat{i}_q \\ \hat{i}_0 \end{bmatrix} + \omega_e \begin{bmatrix} -L_{dq} i_q \\ L_{dq} i_d + \psi_{\mathrm{f}} \\ 0 \end{bmatrix} + \begin{bmatrix} \hat{f}_d \\ \hat{f}_q \\ \hat{f}_0 \end{bmatrix} + \begin{bmatrix} I_{dsmo} \\ I_{qsmo} \\ I_{0smo} \end{bmatrix}$$

$$\frac{\mathrm{d}}{\mathrm{d}t} \begin{bmatrix} \hat{f}_d & \hat{f}_q & \hat{f}_0 \end{bmatrix}^T = \begin{bmatrix} G_d I_{dsmo} & G_q I_{qsmo} & G_0 I_{0smo} \end{bmatrix}^T \tag{18}$$

where $\hat{i}_d$, $\hat{i}_q$, and $\hat{i}_0$ are the estimates of the d-axis, q-axis, and zero-axis currents, respectively, $\hat{f}_d$, $\hat{f}_q$, and $\hat{f}_0$ are the estimates of parameter disturbances f_d, f_q, and f_0, respectively, I_{dsmo}, I_{qsmo}, and I_{0smo} represent sliding mode control function, and G_d, G_q, and G_0 are the gain parameters of the disturbance observer. The current estimation errors and disturbance estimation errors can be expressed as follows:

$$\begin{cases} e_{i_y} = \hat{i}_y - i_y \\ e_{f_y} = \hat{f}_y - f_y \end{cases}, y \in \{d, q, 0\} \tag{19}$$

where e_{i_y} $(y \in \{d, q, 0\})$ represents the errors between the estimated $dq0$-axis currents and the actual feedback currents; e_{f_y} $(y \in \{d, q, 0\})$ represents the errors between the estimated

parameter disturbances and the actual parameter disturbances. Subtracting (16) from (18), the estimation error equations can be obtained as follows:

$$\frac{\mathrm{d}}{\mathrm{d}t}\begin{bmatrix} e_{i_d} \\ e_{i_q} \\ e_{i_0} \end{bmatrix} = \begin{bmatrix} 1/L_{dq} & 0 & 0 \\ 0 & 1/L_{dq} & 0 \\ 0 & 0 & 1/L_0 \end{bmatrix} \times \left(-R_s \begin{bmatrix} e_{i_d} \\ e_{i_q} \\ e_{i_0} \end{bmatrix} - \begin{bmatrix} e_{f_d} \\ e_{f_q} \\ e_{f_0} \end{bmatrix} - \begin{bmatrix} I_{dsmo} \\ I_{qsmo} \\ I_{0smo} \end{bmatrix} \right)$$

$$\frac{\mathrm{d}}{\mathrm{d}t}\begin{bmatrix} e_{f_d} \\ e_{f_q} \\ e_{f_0} \end{bmatrix} = \begin{bmatrix} G_d I_{dsmo} \\ G_q I_{qsmo} \\ G_0 I_{0smo} \end{bmatrix} - \begin{bmatrix} F_d \\ F_q \\ F_0 \end{bmatrix}, \begin{bmatrix} F_d \\ F_q \\ F_0 \end{bmatrix} = \frac{\mathrm{d}}{\mathrm{d}t}\begin{bmatrix} f_d \\ f_q \\ f_0 \end{bmatrix} \tag{20}$$

where F_d, F_q, and F_0 are the variation rates of parameter disturbances f_d, f_q, and f_0, respectively. To ensure the rapid convergence of estimation errors e_{i_d}, e_{i_q}, e_{i_0}, e_{f_d}, e_{f_q}, and e_{f_0}, according to the sliding mode control theory, this article selects e_{i_y} $(y \in \{d, q, 0\})$ as the sliding mode surface, expressed as follows:

$$s_y = e_{i_y} = \hat{i}_y - i_y, y \in \{d, q, 0\}. \tag{21}$$

Moreover, the sliding mode control function is designed based on the exponential reaching law to improve the estimation accuracy of disturbances [35], which can be expressed as follows:

$$\frac{\mathrm{d}s}{\mathrm{d}t} = -\varepsilon \mathrm{sign}(s) - \lambda s, \varepsilon, \lambda > 0 \tag{22}$$

where ε and λ are the reaching law parameters that determine the convergence speed and chattering level. From (20) and (22), considering e_{f_d}, e_{f_q}, and e_{f_0} as the disturbance estimation errors of sliding mode control function, the control function I_{dsmo}, I_{qsmo}, and I_{0smo} can be designed as follows:

$$\begin{cases} I_{dsmo} = (L_{dq}\lambda - R_s)\, e_{i_d} + L_{dq}\varepsilon \mathrm{sign}\,(e_{i_d}) \\ I_{qsmo} = (L_{dq}\lambda - R_s)\, e_{i_q} + L_{dq}\varepsilon \mathrm{sign}\,(e_{i_q}) \\ I_{0smo} = (L_0\lambda - R_s)\, e_{i_0} + L_0\varepsilon \mathrm{sign}\,(e_{i_0}). \end{cases} \tag{23}$$

In order to guarantee the convergence of the estimation errors, the sliding mode control function (23) should satisfy the sliding mode stability condition as follows:

$$\begin{cases} e_{i_d}\frac{\mathrm{d}e_{i_d}}{\mathrm{d}t} = e_{i_d}\left(-\frac{R_s}{L_{dq}}e_{i_d} - \frac{1}{L_{dq}}e_{f_d} - \frac{1}{L_{dq}}I_{dsmo}\right) \le 0 \\ e_{i_q}\frac{\mathrm{d}e_{i_q}}{\mathrm{d}t} = e_{i_q}\left(-\frac{R_s}{L_{dq}}e_{i_q} - \frac{1}{L_{dq}}e_{f_q} - \frac{1}{L_{dq}}I_{qsmo}\right) \le 0 \\ e_{i_0}\frac{\mathrm{d}e_{i_0}}{\mathrm{d}t} = e_{i_0}\left(-\frac{R_s}{L_0}e_{i_0} - \frac{1}{L_0}e_{f_0} - \frac{1}{L_0}I_{0smo}\right) \le 0. \end{cases} \tag{24}$$

Substituting (23) into (24) yields

$$\varepsilon > \max\left(\frac{|e_{f_d}|}{L_{dq}}, \frac{|e_{f_q}|}{L_{dq}}, \frac{|e_{f_0}|}{L_0}\right) \tag{25}$$

which means that the ε should satisfy (25) to ensure the sliding mode stability condition (24) holds. Therefore, the disturbance observer can make the current estimation errors e_{i_d}, e_{i_q}, and e_{i_0} and their derivatives converge to zero in a finite time. Thus, the error equation (20) can be simplified as follows:

$$\frac{\mathrm{d}}{\mathrm{d}t}\begin{bmatrix} e_{f_d} \\ e_{f_q} \\ e_{f_0} \end{bmatrix} + \begin{bmatrix} G_d e_{f_d} \\ G_q e_{f_q} \\ G_0 e_{f_0} \end{bmatrix} + \begin{bmatrix} F_d \\ F_q \\ F_0 \end{bmatrix} = \begin{bmatrix} 0 \\ 0 \\ 0 \end{bmatrix}. \tag{26}$$

Therefore, the solution for disturbance estimation errors e_{f_d}, e_{f_q}, and e_{f_0} are given by

$$e_{f_y} = e^{-G_y t}\left(C + \int F_y e^{G_y t}\mathrm{d}t\right), y \in \{d, q, 0\} \tag{27}$$

where C is a constant. It can be seen from (27) that gain parameters G_d, G_q, and G_0 should be positive to ensure the convergence of disturbance estimation errors. Moreover, the above analysis proves that the designed disturbance observer (18) is stable with appropriate control parameters ε, G_d, G_q, and G_0.

For digital implementation [36], the expression of the disturbance observer (18) should be discretized as follows:

$$\begin{bmatrix} \hat{i}_d(k+1) \\ \hat{i}_q(k+1) \\ \hat{i}_0(k+1) \end{bmatrix} = M \begin{bmatrix} \hat{i}_d(k) \\ \hat{i}_q(k) \\ \hat{i}_0(k) \end{bmatrix} + B\left(\begin{bmatrix} u_d(k) \\ u_q(k) \\ u_0(k) \end{bmatrix} - \begin{bmatrix} \hat{f}_d(k) \\ \hat{f}_q(k) \\ \hat{f}_0(k) \end{bmatrix} - \begin{bmatrix} I_{dsmo}(k) \\ I_{qsmo}(k) \\ I_{0smo}(k) \end{bmatrix}\right) + T_c\omega_e(k)\begin{bmatrix} i_q(k) \\ -i_d(k) \\ 0 \end{bmatrix} + E(k)$$

$$\begin{bmatrix} \hat{f}_d(k+1) \\ \hat{f}_q(k+1) \\ \hat{f}_0(k+1) \end{bmatrix} = \begin{bmatrix} \hat{f}_d(k) \\ \hat{f}_q(k) \\ \hat{f}_0(k) \end{bmatrix} + T_c\begin{bmatrix} G_d I_{dsmo}(k) \\ G_q I_{qsmo}(k) \\ G_0 I_{0smo}(k) \end{bmatrix}, G_d, G_q, G_0 \in R^+$$

$$M = \mathrm{diag}\begin{bmatrix} 1 - \frac{T_c R_s}{L_{dq}} & 1 - \frac{T_c R_s}{L_{dq}} & 1 - \frac{T_c R_s}{L_0} \end{bmatrix} \tag{28}$$

where $\hat{i}_d(k+1)$, $\hat{i}_q(k+1)$, and $\hat{i}_0(k+1)$ are the $(k+1)$th instant d-, q-, and zero-axes currents estimated by the observer, respectively. $\hat{f}_d(k+1)$, $\hat{f}_q(k+1)$, and $\hat{f}_0(k+1)$ are the estimates of parameter disturbances at the $(k+1)$th instant. The $I_{dsmo}(k)$, $I_{qsmo}(k)$, and $I_{0smo}(k)$ can be expressed as follows:

$$\begin{cases} I_{dsmo}(k) = (L_{dq}\lambda - R_s)\, e_{i_d}(k) + L_{dq}\varepsilon \mathrm{sign}\,(e_{i_d}(k)) \\ I_{qsmo}(k) = (L_{dq}\lambda - R_s)\, e_{i_q}(k) + L_{dq}\varepsilon \mathrm{sign}\,(e_{i_q}(k)) \\ I_{0smo}(k) = (L_0\lambda - R_s)\, e_{i_0}(k) + L_0\varepsilon \mathrm{sign}\,(e_{i_0}(k)) \end{cases} \tag{29}$$

with

$$e_{i_y}(k) = \hat{i}_y(k) - i_y(k), y \in \{d, q, 0\}. \tag{30}$$

Therefore, the output of observer at the kth instant is

$$\begin{bmatrix} \hat{i}_d(k) \\ \hat{i}_q(k) \\ \hat{i}_0(k) \end{bmatrix} = M \begin{bmatrix} \hat{i}_d(k-1) \\ \hat{i}_q(k-1) \\ \hat{i}_0(k-1) \end{bmatrix}$$

$$+B\left(\begin{bmatrix}u_d(k-1)\\u_q(k-1)\\u_0(k-1)\end{bmatrix}-\begin{bmatrix}\hat{f}_d(k-1)\\\hat{f}_q(k-1)\\\hat{f}_0(k-1)\end{bmatrix}-\begin{bmatrix}I_{dsmo}(k-1)\\I_{qsmo}(k-1)\\I_{0smo}(k-1)\end{bmatrix}\right)$$

$$+T_c\omega_e(k-1)\begin{bmatrix}i_q(k-1)\\-i_d(k-1)\\0\end{bmatrix}+E(k-1)$$

$$\begin{bmatrix}\hat{f}_d(k)\\\hat{f}_q(k)\\\hat{f}_0(k)\end{bmatrix}=\begin{bmatrix}\hat{f}_d(k-1)\\\hat{f}_q(k-1)\\\hat{f}_0(k-1)\end{bmatrix}+T_c\begin{bmatrix}G_dI_{dsmo}(k-1)\\G_qI_{qsmo}(k-1)\\G_0I_{0smo}(k-1)\end{bmatrix}$$

$$\begin{cases}I_{dsmo}(k-1)= & (L_{dq}\lambda-R_s)\,e_{id}(k-1)\\ & +L_{dq}\varepsilon\mathrm{sign}\,(e_{id}(k-1))\\ I_{qsmo}(k-1)= & (L_{dq}\lambda-R_s)\,e_{iq}(k-1)\\ & +L_{dq}\varepsilon\mathrm{sign}\,(e_{iq}(k-1))\\ I_{0smo}(k-1)= & (L_0\lambda-R_s)\,e_{i0}(k-1)\\ & +L_0\varepsilon\mathrm{sign}\,(e_{i0}(k-1))\,.\end{cases}\tag{31}$$

Subtracting (31) from (28) yields

$$\begin{bmatrix}\Delta\hat{i}_d(k+1)\\\Delta\hat{i}_q(k+1)\\\Delta\hat{i}_0(k+1)\end{bmatrix}=M\begin{bmatrix}\Delta\hat{i}_d(k)\\\Delta\hat{i}_q(k)\\\Delta\hat{i}_0(k)\end{bmatrix}$$

$$+B\left(\begin{bmatrix}\Delta u_d(k)\\\Delta u_q(k)\\\Delta u_0(k)\end{bmatrix}-\begin{bmatrix}\Delta\hat{f}_d(k)\\\Delta\hat{f}_q(k)\\\Delta\hat{f}_0(k)\end{bmatrix}-\begin{bmatrix}\Delta I_{dsmo}(k)\\\Delta I_{qsmo}(k)\\\Delta I_{0smo}(k)\end{bmatrix}\right)$$

$$+T_c\omega_e(k)\begin{bmatrix}\Delta i_q(k)\\-\Delta i_d(k)\\0\end{bmatrix}$$

$$\begin{bmatrix}\Delta\hat{f}_d(k+1)\\\Delta\hat{f}_q(k+1)\\\Delta\hat{f}_0(k+1)\end{bmatrix}=\begin{bmatrix}\Delta\hat{f}_d(k)\\\Delta\hat{f}_q(k)\\\Delta\hat{f}_0(k)\end{bmatrix}+T_c\begin{bmatrix}G_d\Delta I_{dsmo}(k)\\G_q\Delta I_{qsmo}(k)\\G_0\Delta I_{0smo}(k)\end{bmatrix}\tag{32}$$

with

$$\begin{cases}\Delta\hat{i}_y(k)=\hat{i}_y(k)-\hat{i}_y(k-1)\\ \Delta\hat{i}_y(k+1)=\hat{i}_y(k+1)-\hat{i}_y(k)\\ \Delta\hat{f}_y(k)=\hat{f}_y(k)-\hat{f}_y(k-1)\\ \Delta\hat{f}_y(k+1)=\hat{f}_y(k+1)-\hat{f}_y(k)\\ \Delta u_y(k)=u_y(k)-u_y(k-1)\end{cases},\ y\in\{d,q,0\}\tag{33}$$

$$\begin{cases}\Delta I_{dsmo}(k)=I_{dsmo}(k)-I_{dsmo}(k-1)\\ \Delta I_{qsmo}(k)=I_{qsmo}(k)-I_{qsmo}(k-1)\\ \Delta I_{0smo}(k)=I_{0smo}(k)-I_{0smo}(k-1)\,.\end{cases}\tag{34}$$

It can be seen from (32)–(34) that the proposed SMDO eliminates the flux linkage ψ_f, which has a significant impact on the current and disturbance estimation. The structure diagram of the proposed SMDO is shown in Fig. 4.

C. IDPCC + SMDO Method

By replacing the sampled currents in incremental prediction model (14) with d-, q-, and zero-axes currents estimated by the proposed SMDO at the $(k+1)$th instant and compensating parameter disturbances with the estimated incremental disturbances of observer, the proposed incremental DPCC with sliding mode disturbance observer method can be expressed as

$$\begin{bmatrix}u_d^*\\u_q^*\\u_0^*\end{bmatrix}=B^{-1}\left(\begin{bmatrix}i_d^*(k+1)\\i_q^*(k+1)\\i_0^*(k+1)\end{bmatrix}-\begin{bmatrix}\hat{i}_d(k+1)\\\hat{i}_q(k+1)\\\hat{i}_0(k+1)\end{bmatrix}-A(k)\begin{bmatrix}\Delta\hat{i}_d(k+1)\\\Delta\hat{i}_q(k+1)\\\Delta\hat{i}_0(k+1)\end{bmatrix}\right)+\begin{bmatrix}\Delta\hat{f}_d(k+1)\\\Delta\hat{f}_q(k+1)\\\Delta\hat{f}_0(k+1)\end{bmatrix}+\begin{bmatrix}u_d(k-1)\\u_q(k-1)\\u_0(k-1)\end{bmatrix}.\tag{35}$$

The structure of the proposed IDPCC + SMDO method for PMSM drive systems using four-leg inverters is shown in Fig. 5. The sampled currents $i_d(k)$, $i_q(k)$, and $i_0(k)$ are utilized to derive the predictive currents and disturbance values through the proposed SMDO, which can effectively suppress the impact of resistance and inductance parameter mismatches on the incremental prediction model. In contrast to the DPCC method, the proposed IDPCC + SMDO method introduces an additional disturbance estimation and compensation process. While this slightly increases the computational burden, the benefit is clear,

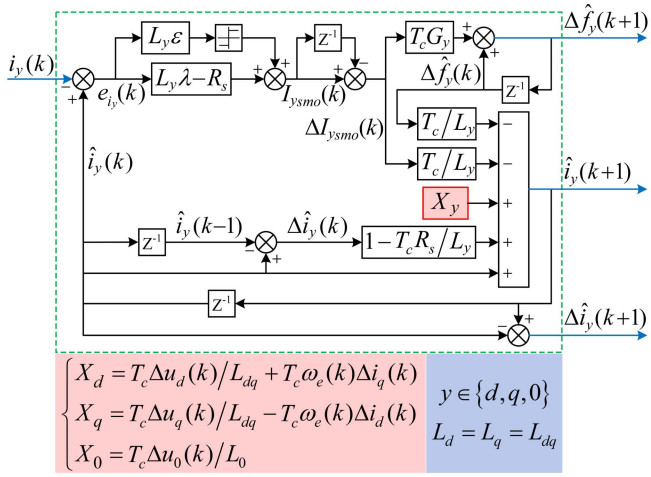

Fig. 4. Structural diagram of the proposed incremental form of SMDO.

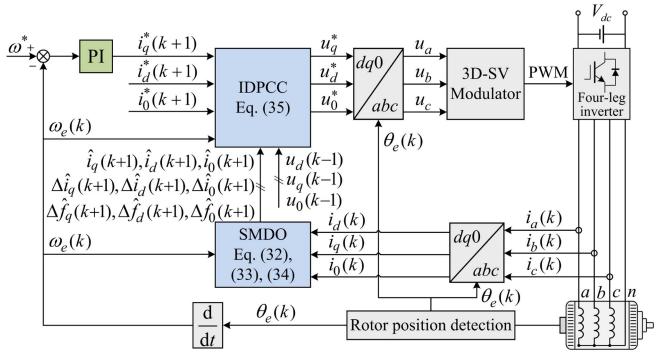

Fig. 5. Control diagram of the proposed IDPCC + SMDO method.

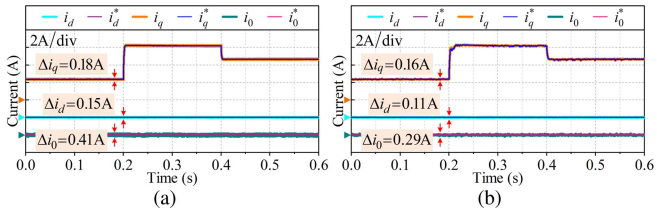

Fig. 6. Simulation performance of the two methods in healthy operation mode at 600 r/min without parameter mismatch ($\Delta R_s = 0$, $\Delta L_{dq} = 0$, $\Delta L_0 = 0$ and $\Delta\psi_{\mathrm{f}} = 0$). (a) DPCC. (b) IDPCC + SMDO.

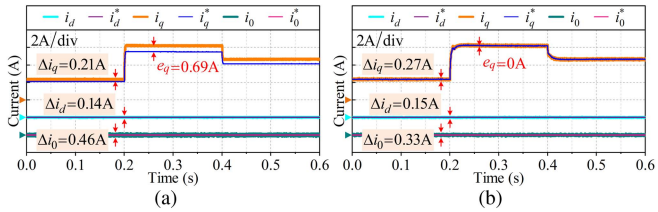

Fig. 7. Simulation performance of the two methods in healthy operation mode at 600 r/min under 10 times resistance ($\Delta R_s = 9R_s$, $\Delta L_{dq} = 0$, $\Delta L_0 = 0$, and $\Delta\psi_{\mathrm{f}} = 0$). (a) DPCC. (b) IDPCC + SMDO.

as it significantly enhances the controller's robustness to parameter mismatches. In addition, the proposed SMDO is capable of compensating for the one-step delay inherent in digital controllers.

IV. Performance Simulation

In this section, the simulation modeling and analysis are implemented into a surface-mounted PMSM to verify the effectiveness of the proposed IDPCC + SMDO method in mitigating the influence of motor parameter mismatches. The simulation of conventional DPCC method is also conducted to compare the control performance of the proposed method in healthy and open-phase fault-tolerant mode of the tested PMSM. Since the motor parameters cannot be set arbitrarily, the corresponding parameter mismatches are simulated by modifying the parameter values used in the prediction model. The major parameters of tested machine are listed in Table I.

A. Control Performance Comparison Under Healthy Mode

When the PMSM drive system is in healthy operation mode, the reference of zero-axis current i_0 should be set to 0 A. The load torque changes are uniformly set to change from 3 to 8 N·m at the time instant $t_1 = 0.2$ s and then to 6 N· m at the time instant $t_2 = 0.4$ s. The target speed is set to 600 r/min, and the control frequency used in the simulation is 20 kHz, while the speed loop sampling frequency is 2 kHz.

Fig. 6 illustrates a comparison of the current dynamic performance between the two methods under conditions of no parameter mismatch ($\Delta R_s = 0$, $\Delta L_{dq} = 0$, $\Delta L_0 = 0$, and $\Delta\psi_{\mathrm{f}} = 0$). Both methods accurately track the current reference, but the proposed IDPCC + SMDO method exhibits lower current ripple than the conventional DPCC method, particularly in the zero-axis current ripple. This is because the proposed SMDO can compensate for the effect of one-step delay, which has a more pronounced impact on the zero-axis current due to the small L_0. The simulation results of the $dq0$-axis current responses under various parameter mismatch conditions are presented in Figs. 7–14.

The current dynamic performance comparison of the two methods under 10 and 0.1 times resistance mismatch are shown in Figs. 7 and 8, respectively. Under resistance mismatch, the q-axis current of the DPCC method fails to accurately track the reference, whereas the proposed IDPCC + SMDO method effectively eliminates the static error in the q-axis current.

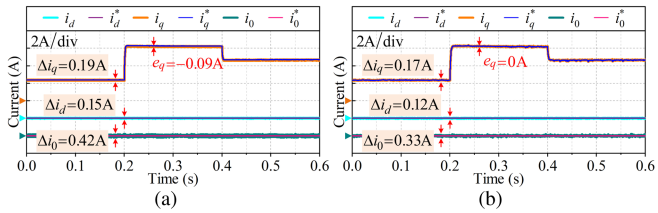

Fig. 8. Simulation performance of the two methods in healthy operation mode at 600 r/min under 0.1 times resistance ($\Delta R_s = -0.9R_s$, $\Delta L_{dq} = 0$, $\Delta L_0 = 0$, and $\Delta\psi_{\mathrm{f}} = 0$). (a) DPCC. (b) IDPCC + SMDO.

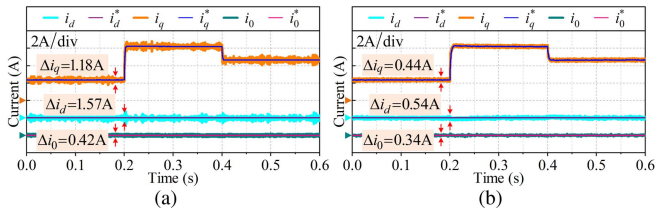

Fig. 9. Simulation performance of the two methods in healthy operation mode at 600r/min under 2 times dq-axis inductance ($\Delta R_s = 0$, $\Delta L_{dq} = L_{dq}$, $\Delta L_0 = 0$, and $\Delta\psi_{\mathrm{f}} = 0$). (a) DPCC. (b) IDPCC + SMDO.

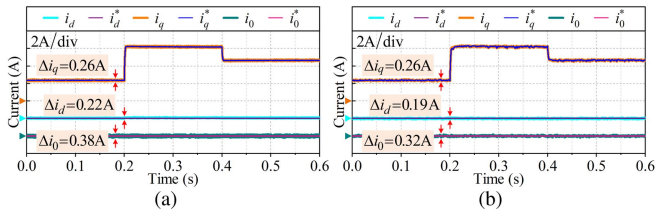

Fig. 10. Simulation performance of the two methods in healthy operation mode at 600 r/min under 0.5 times dq-axis inductance ($\Delta R_s = 0$, $\Delta L_{dq} = -0.5L_{dq}$, $\Delta L_0 = 0$, and $\Delta\psi_{\mathrm{f}} = 0$). (a) DPCC. (b) IDPCC + SMDO.

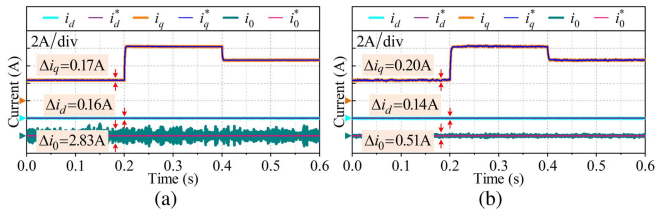

Fig. 11. Simulation performance of the two methods in healthy operation mode at 600 r/min under 2 times zero-axis inductance ($\Delta R_s = 0$, $\Delta L_{dq} = 0$, $\Delta L_0 = L_0$ and $\Delta\psi_{\mathrm{f}} = 0$). (a) DPCC. (b) IDPCC + SMDO.

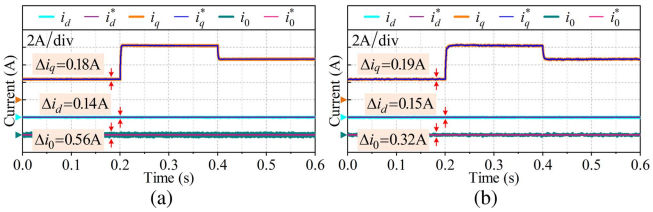

Fig. 12. Simulation performance of the two methods in healthy operation mode at 600 r/min under 0.5 times zero-axis inductance ($\Delta R_s = 0, \Delta L_{dq} = 0, \Delta L_0 = -0.5L_0$, and $\Delta\psi_{\mathrm{f}} = 0$). (a) DPCC. (b) IDPCC + SMDO.

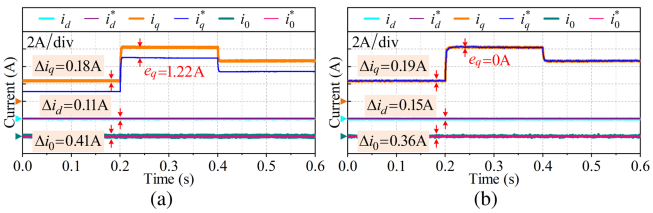

Fig. 13. Simulation performance of the two methods in healthy operation mode at 600 r/min under 2 times flux linkage ($\Delta R_s = 0, \Delta L_{dq} = 0, \Delta L_0 = 0$, and $\Delta\psi_{\mathrm{f}} = \psi_{\mathrm{f}}$). (a) DPCC. (b) IDPCC + SMDO.

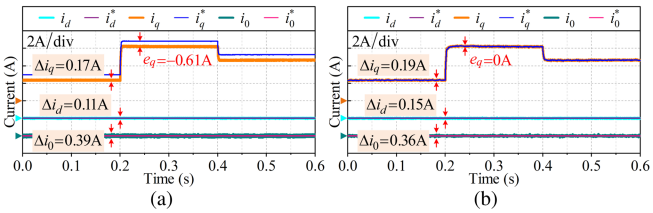

Fig. 14. Simulation performance of the two methods in healthy operation mode at 600 r/min under 0.5 times flux linkage ($\Delta R_s = 0, \Delta L_{dq} = 0, \Delta L_0 = 0$, and $\Delta\psi_{\mathrm{f}} = -0.5\psi_{\mathrm{f}}$). (a) DPCC. (b) IDPCC + SMDO.

Figs. 9 and 10 present the current responses under 2 and 0.5 times dq-axis inductance mismatch, respectively. It can be observed that when the dq-axis inductance value used in the prediction model is larger than the actual value, there is no tracking error in the $dq0$-axis currents, while the dq-axis current ripple may increase significantly. However, the proposed IDPCC + SMDO method effectively suppresses this current ripple by compensating for parameter mismatches. A similar situation is observed in the current dynamic performance comparison under 2 and 0.5 times zero-axis inductance mismatch, as shown in Figs. 11 and 12, respectively. Under 2 times zero-axis inductance mismatch, the zero-axis current of the DPCC method oscillates violently, whereas the IDPCC + SMDO method suppresses these oscillations, contributing to smoother output torque. In addition, the permanent magnet flux linkage mismatch introduces a static error in the q-axis current of the DPCC method. In contrast, the proposed IDPCC + SMDO method completely eliminates the influence of flux linkage by employing the incremental prediction model, as demonstrated in Figs. 13 and 14.

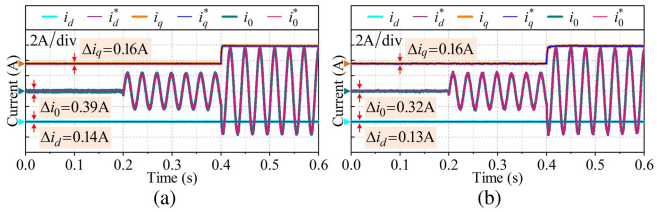

Fig. 15. Simulation performance of the two methods in open-phase fault-tolerant mode at 500 r/min without parameter mismatch ($\Delta R_s = 0, \Delta L_{dq} = 0, \Delta L_0 = 0$, and $\Delta\psi_{\mathrm{f}} = 0$). (a) DPCC. (b) IDPCC + SMDO.

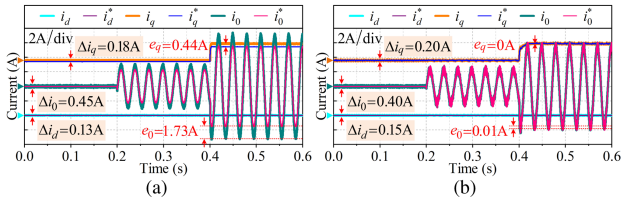

Fig. 16. Simulation performance of the two methods in open-phase fault-tolerant mode at 500 r/min under 10 times resistance ($\Delta R_s = 9R_s, \Delta L_{dq} = 0, \Delta L_0 = 0$, and $\Delta\psi_{\mathrm{f}} = 0$). (a) DPCC. (b) IDPCC + SMDO.

B. Control Performance Comparison Under Open-Phase Fault-Tolerant Mode

When the PMSM drive system is in open-phase fault-tolerant operation mode, the reference of zero-axis current i_0 should be adjusted to (2)–(4) according to the position of open-phase fault. In this simulation study, the open-phase fault occurs in the phase A is taken as an example. The open-phase fault occurs at the time instant $t_2 = 0.2$s. The load torque changes are uniformly set to change from 2 to 5 N· m at the time instant $t_2 = 0.4$ s. The target speed is set to 500 r/min, and the control frequency used in the simulation is 20 kHz, while the speed loop sampling frequency is 2 kHz.

Fig. 15 presents the current dynamic performance comparison of the two methods under open-phase fault-tolerant operation mode without parameter mismatch ($\Delta R_s = 0$, $\Delta L_{dq} = 0$, $\Delta L_0 = 0$, and $\Delta\psi_{\mathrm{f}} = 0$). Both methods exhibit fast current dynamic response and can accurately track the current reference, particularly for the zero-axis ac current reference. However, the proposed IDPCC + SMDO method can effectively mitigate the influence of one-step delay on motor control, resulting in lower current ripple compared to the conventional DPCC method.

Figs. 16 and 17 illustrate a comparative analysis of the current dynamic performance of the two methods under 10 and 0.1 times resistance mismatch, respectively. In the DPCC method, both the q-axis current i_q and the zero-axis current i_0 fail to accurately track their respective reference values under resistance mismatch. Specifically, the amplitude of the actual i_0 significantly deviates from the reference current i_0^* under open-phase fault-tolerant mode with 10 times resistance mismatch. In contrast, the proposed IDPCC + SMDO method effectively mitigates the tracking errors of both the q- and zero-axes currents, ensuring accurate alignment with their reference currents by compensating for disturbances arising from parameter mismatches.

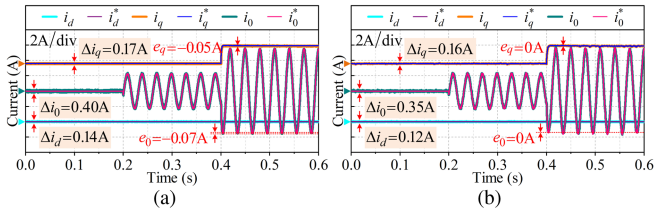

Fig. 17. Simulation performance of the two methods in open-phase fault-tolerant mode at 500 r/min under 0.1 times resistance ($\Delta R_s = -0.9R_s$, $\Delta L_{dq} = 0$, $\Delta L_0 = 0$, and $\Delta\psi_{\mathrm{f}} = 0$). (a) DPCC. (b) IDPCC + SMDO.

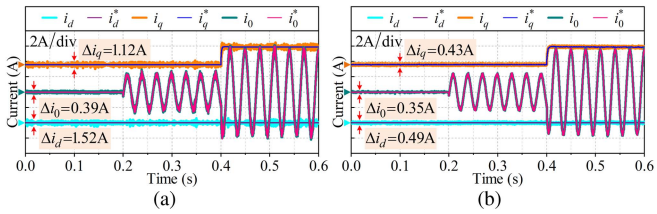

Fig. 18. Simulation performance of the two methods in open-phase fault-tolerant mode at 500 r/min under 2 times dq-axis inductance ($\Delta R_s = 0$, $\Delta L_{dq} = L_{dq}$, $\Delta L_0 = 0$, and $\Delta\psi_{\mathrm{f}} = 0$). (a) DPCC. (b) IDPCC + SMDO.

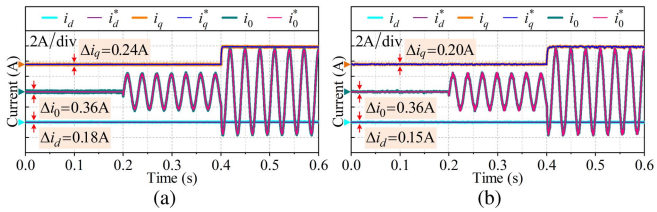

Fig. 19. Simulation performance of the two methods in open-phase fault-tolerant mode at 500 r/min under 0.5 times dq-axis inductance ($\Delta R_s = 0$, $\Delta L_{dq} = -0.5L_{dq}$, $\Delta L_0 = 0$, and $\Delta\psi_{\mathrm{f}} = 0$). (a) DPCC. (b) IDPCC + SMDO.

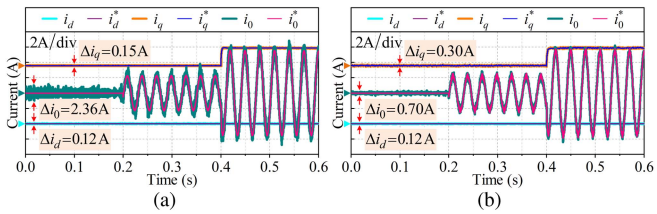

Fig. 20. Simulation performance of the two methods in open-phase fault-tolerant mode at 500 r/min under 2 times zero-axis inductance ($\Delta R_s = 0$, $\Delta L_{dq} = 0$, $\Delta L_0 = L_0$ and $\Delta\psi_{\mathrm{f}} = 0$). (a) DPCC. (b) IDPCC + SMDO.

Figs. 18 and 19 demonstrate that the DPCC method exhibits significant sensitivity to dq-axis inductance mismatch, with the $dq0$-axis currents showing obvious oscillations when the L_{dq} used in the prediction model exceeds the actual inductance value. A similar phenomenon is observed under zero-axis inductance L_0 mismatch, the difference is that L_0 mismatch mainly affects the ripple of zero-axis current i_0, as shown in Figs. 20 and 21. However, the proposed IDPCC + SMDO method can effectively suppress the current ripple induced by inductance mismatches,

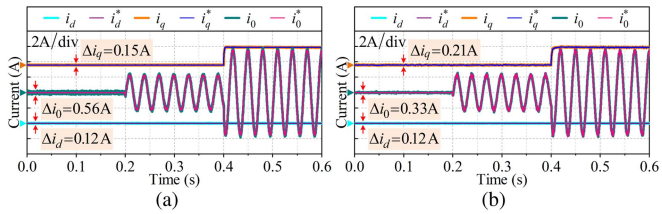

Fig. 21. Simulation performance of the two methods in open-phase fault-tolerant mode at 500 r/min under 0.5 times zero-axis inductance ($\Delta R_s = 0$, $\Delta L_{dq} = 0$, $\Delta L_0 = -0.5L_0$, and $\Delta\psi_{\mathrm{f}} = 0$). (a) DPCC. (b) IDPCC + SMDO.

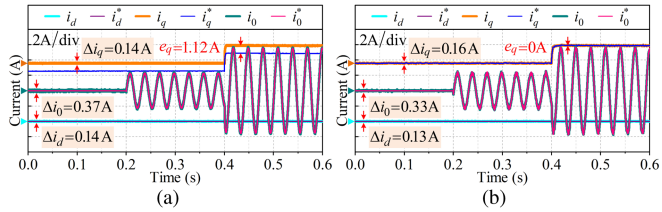

Fig. 22. Simulation performance of the two methods in open-phase fault-tolerant mode at 500 r/min under 2 times flux linkage ($\Delta R_s = 0$, $\Delta L_{dq} = 0$, $\Delta L_0 = 0$, and $\Delta\psi_{\mathrm{f}} = \psi_{\mathrm{f}}$). (a) DPCC. (b) IDPCC + SMDO.

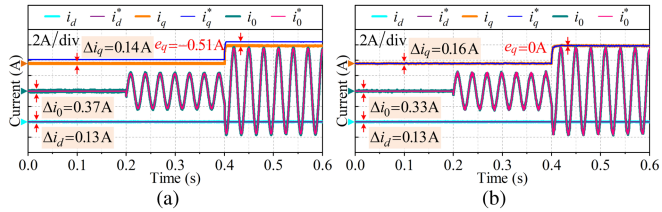

Fig. 23. Simulation performance of the two methods in open-phase fault-tolerant mode at 500 r/min under 0.5 times flux linkage ($\Delta R_s = 0$, $\Delta L_{dq} = 0$, $\Delta L_0 = 0$, and $\Delta\psi_{\mathrm{f}} = -0.5\psi_{\mathrm{f}}$). (a) DPCC. (b) IDPCC + SMDO.

thereby reducing the torque ripple resulting from current prediction error.

In addition, the current dynamic performance comparison of the two methods under 2 and 0.5 times flux linkage mismatch are shown in Figs. 22 and 23, respectively. Similar to the healthy operation mode, the proposed IDPCC + SMDO method completely eliminates the effects of permanent magnet flux linkage mismatch in the open-phase fault-tolerant operation mode by employing the incremental prediction model.

In summary, the comparison and analysis of the above simulation results demonstrate that the proposed IDPCC + SMDO method has better current control performance under various motor parameter mismatches than conventional DPCC method. Disturbance compensation effectively mitigates the negative impact of parameter mismatches and one-step delay on predictive control performance, thereby greatly enhancing the parameter robustness of the controller.

V. Experimental Results

To validate the effectiveness of IDPCC + SMDO method proposed in this article, one experimental platform has been developed for the control performance evaluation, as depicted

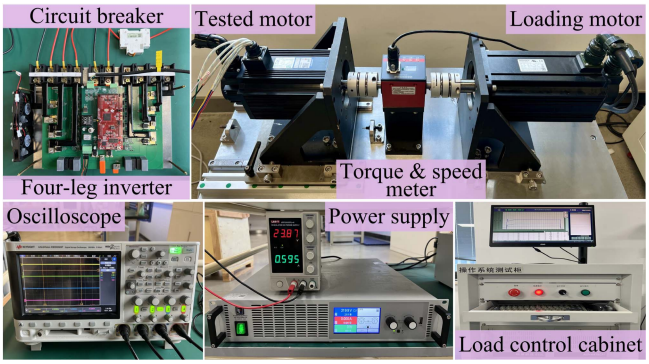

Fig. 24. Experimental setup for evaluating the contol performance of PMSM drive system using a four-leg inverter.

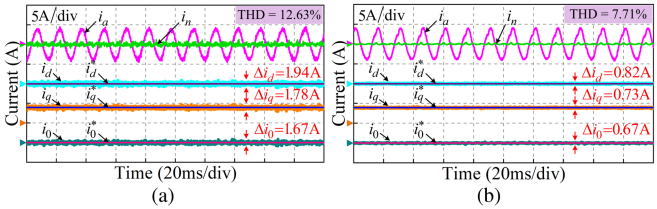

Fig. 25. Experimental data of the two methods in healthy operation mode at 1000 r/min and 5 N· m without parameter mismatch ($\Delta R_s = 0$, $\Delta L_{dq} = 0$, $\Delta L_0 = 0$, and $\Delta\psi_{\rm f} = 0$). (a) DPCC. (b) IDPCC + SMDO.

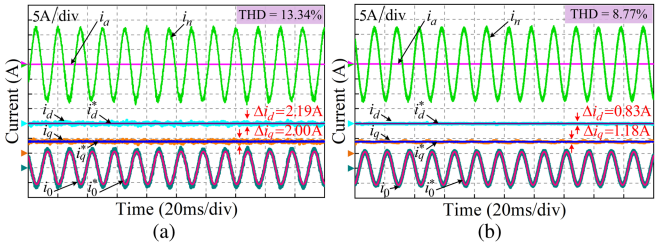

Fig. 26. Experimental data of the two methods in open-phase fault-tolerant operation mode at 1000 r/min and 5 N·m without parameter mismatch ($\Delta R_s = 0$, $\Delta L_{dq} = 0$, $\Delta L_0 = 0$, and $\Delta\psi_{\rm f} = 0$). (a) DPCC. (b) IDPCC + SMDO.

in Fig. 24. The experimental platform consists of a tested PMSM, a torque-speed meter, a loading motor, a load control cabinet, an oscilloscope, a dc power supply and a four-leg inverter. A circuit breaker is employed to connect the A-phase of tested machine and inverter, which can simulate the open-phase fault when in the disconnected state. The algorithm execution logic is constructed based on the DSP TMS320F28379D chip, and the major parameters of tested machine are provided in Table I. The dc-bus voltage of tested PMSM in experiments is set to 220 V, and the control frequency adopted by the system is fixed at 20 kHz. The parameters of the sliding mode disturbance observer are set as follows: $\varepsilon = 1000$, $\lambda = 3150$, $G_d = G_q = 100$, and $G_0 = 2000$, ensuring the asymptotic stability of the proposed SMDO.

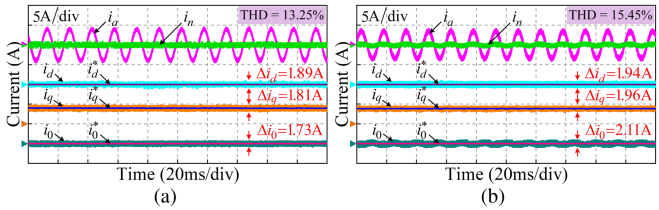

Fig. 27. Experimental data of the PID and FCS-MPCC methods in healthy operation mode at 1000 r/min and 5 N·m without parameter mismatch ($\Delta R_s = 0$, $\Delta L_{dq} = 0$, $\Delta L_0 = 0$, and $\Delta\psi_{\rm f} = 0$). (a) PID. (b) FCS-MPCC.

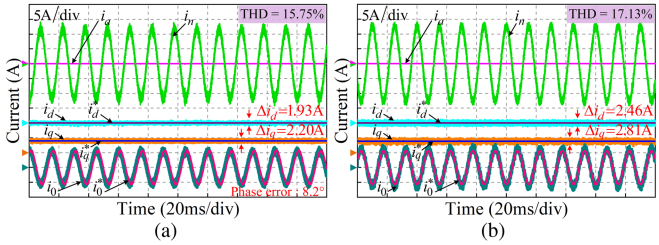

Fig. 28. Experimental data of the PID and FCS-MPCC methods in open-phase fault-tolerant operation mode at 1000 r/min and 5 N·m without parameter mismatch ($\Delta R_s = 0$, $\Delta L_{dq} = 0$, $\Delta L_0 = 0$, and $\Delta\psi_{\rm f} = 0$). (a) PID. (b) FCS-MPCC.

A. *Steady-State Performance Comparison*

Figs. 25 and 26 present the experimental outcomes of DPCC and the proposed IDPCC + SMDO methods in both healthy and open-phase fault-tolerant operation modes, respectively. The experimental data are all obtained at the speed of 1000 r/min and the torque output of 5 N·m, with no parameter mismatch. It is evident that the $dq0$-axis currents for both methods accurately track the reference currents, and the total harmonic distortion (THD) of the phase current is similar in both the healthy and open-phase fault-tolerant operation modes. However, the proposed IDPCC + SMDO method demonstrates lower $dq0$-axis current ripple and phase current THD compared to the conventional DPCC method, which is advantageous for achieving smooth output torque in PMSM drive systems. To further validate the current control performance of the proposed IDPCC + SMDO method, this study presents comparative experimental results with conventional PID and FCS-MPCC methods in both healthy and open-phase fault-tolerant operation modes, as shown in Figs. 27 and 28, respectively. The control frequency of the PID method is set at 20 kHz, while that of the FCS-MPCC method is 50 kHz. When the PMSM drive system is in healthy operation mode, both PID and FCS-MPCC methods can accurately track the reference currents; however, their $dq0$-axis current ripples and A-phase current THD are notably higher than those achieved by proposed IDPCC + SMDO method. When the PMSM drive system is in open-phase fault-tolerant operation mode, the PID method exhibits an 8.2° phase difference between the zero-axis current and its reference. Furthermore, the N-phase current THD and $dq0$-axis current ripple of both PID and FCS-MPCC increase significantly in fault-tolerant operation mode, remaining considerably higher than those of the proposed IDPCC + SMDO method.

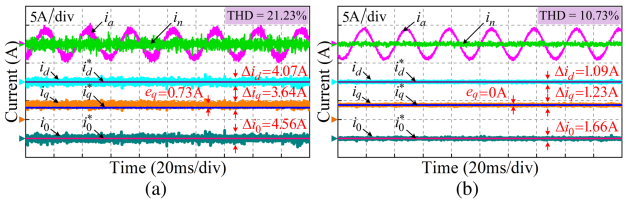

Fig. 29. Experimental data of the two methods in healthy operation mode at 500 r/min and 5 N·m under simultaneous multiparameter mismatches ($\Delta R_s = 9R_s$, $\Delta L_{dq} = L_{dq}$, $\Delta L_0 = L_0$, and $\Delta\psi_{\rm f} = \psi_{\rm f}$). (a) DPCC. (b) IDPCC + SMDO.

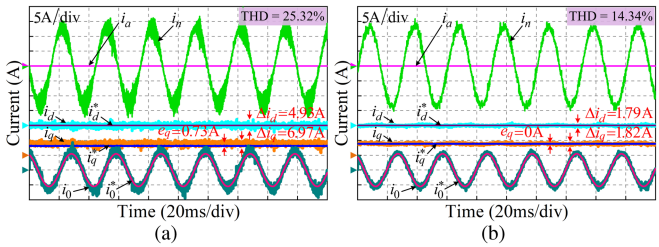

Fig. 30. Experimental data of the two methods in open-phase fault-tolerant operation mode at 500 r/min and 5N·m under simultaneous multiparameter mismatches ($\Delta R_s = 9R_s$, $\Delta L_{dq} = L_{dq}$, $\Delta L_0 = L_0$, and $\Delta\psi_{\rm f} = \psi_{\rm f}$). (a) DPCC. (b) IDPCC + SMDO.

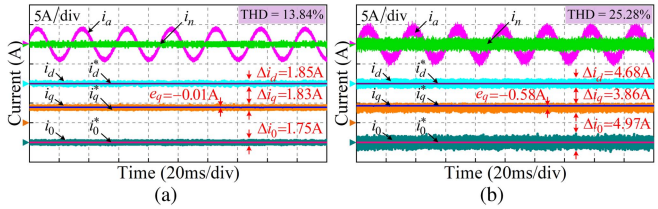

Fig. 31. Experimental data of the PID and FCS-MPCC methods in healthy operation mode at 500 r/min and 5 N·m under simultaneous multiparameter mismatches ($\Delta R_s = 9R_s$, $\Delta L_{dq} = L_{dq}$, $\Delta L_0 = L_0$, and $\Delta\psi_{\rm f} = \psi_{\rm f}$). (a) PID. (b) FCS-MPCC.

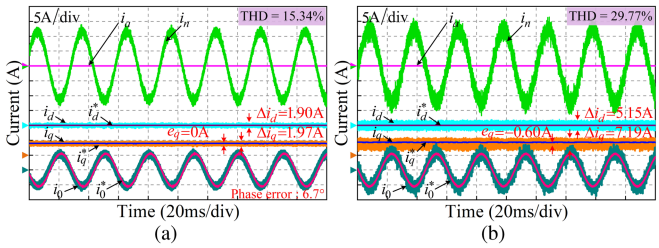

Fig. 32. Experimental data of the PID and FCS-MPCC methods in open-phase fault-tolerant operation mode at 500 r/min and 5 N·m under simultaneous multiparameter mismatches ($\Delta R_s = 9R_s$, $\Delta L_{dq} = L_{dq}$, $\Delta L_0 = L_0$, and $\Delta\psi_{\rm f} = \psi_{\rm f}$). (a) PID. (b) FCS-MPCC.

The control performance of DPCC and the proposed IDPCC + SMDO methods under a single parameter mismatch has been analyzed in the previous simulation study. The results indicate that $dq0$-axis current ripple and static error usually increase significantly when the parameter values used in the current prediction model are larger than their actual counterparts. However, in practical PMSM drive systems, parameter mismatches often occur simultaneously across multiple parameters. To conduct a more comprehensive analysis of control performance between the proposed IDPCC + SMDO method and conventional DPCC method under simultaneous multiparameter mismatches in this section, the parameter mismatch conditions are set to $\Delta R_s = 9R_s$, $\Delta L_{dq} = L_{dq}$, $\Delta L_0 = L_0$, and $\Delta\psi_{\rm f} = \psi_{\rm f}$. The performance comparison of the two methods is then conducted at the speed of 500 r/min and the torque output of 5 N·m.

Fig. 29 shows a comparison of the steady-state performance between the DPCC and the proposed IDPCC + SMDO methods in healthy operation mode under simultaneous multiparameter mismatches. The experimental results reveal that the multiparameter mismatches lead to a significant increase in the A-phase current THD for the DPCC method, from 12.63% at 1000 r/min to 21.23% at 500 r/min. In addition, the current ripples in the d-, q-, and zero-axes rise from 1.94 to 4.07 A, 1.78 to 3.64 A, and 1.67 to 4.56 A, respectively. Moreover, the static error between the actual q-axis current and the reference current caused by multiparameter mismatches reaches 0.73 A. However, the steady-state performance of the proposed IDPCC + SMDO method, as shown in Fig. 29(b), is almost unaffected by the multiparameter mismatches, thereby achieving more satisfactory control performance.

A similar situation is observed in open-phase fault-tolerant operation mode under simultaneous multiparameter mismatches, as shown in Fig. 30. The N-phase current THD for the conventional DPCC method increases from 13.34% at 1000 r/min to 25.32% at 500 r/min. The d-axis current ripple rises from 2.19 to 4.93 A, and the q-axis current ripple increases from 2 to 6.97 A. Furthermore, the zero-axis current ripple also increases substantially in open-phase fault-tolerant operation mode under multiparameter mismatches. In contrast, the proposed IDPCC + SMDO method effectively suppresses the N-phase current THD and $dq0$-axis current ripple caused by parameter mismatches, while eliminating the static error in the q-axis current, as shown in Fig. 30(b).

This study also investigates the current control performance of conventional PID and FCS-MPCC methods under simultaneous multiparameter mismatches in both healthy and open-phase fault-tolerant operation modes, as illustrated in Figs. 31 and 32, respectively. Since the PID controller does not rely on the PMSM mathematical model, its phase current THD and dq-axis current ripple remain largely unaffected by parameter mismatches. Meanwhile, the phase difference between the zero-axis current and its reference slightly decreases from 8.2° at 1000 r/min to 6.7° at 500 r/min, as shown in Figs. 28(a) and 32(a). In contrast, the FCS-MPCC method, similar to the DPCC method, is highly sensitive to parameter mismatches, which result in a substantial increase in both the $dq0$-axis current ripple and phase current THD. Figs. 27(b) and 31(b) demonstrate that under healthy operating conditions, the multiparameter mismatches lead to a significant increase in the A-phase current THD for the FCS-MPCC method, rising from 15.45% at 1000 r/min to 25.28% at 500 r/min. In addition, the current ripples in the d-, q-, and zero-axes rise from 1.94 to 4.68 A, 1.96 to 3.86 A, and 2.11 to 4.97 A, respectively. Moreover, the multiparameter mismatches introduce a steady-state error of −0.58 A between the actual q-axis current

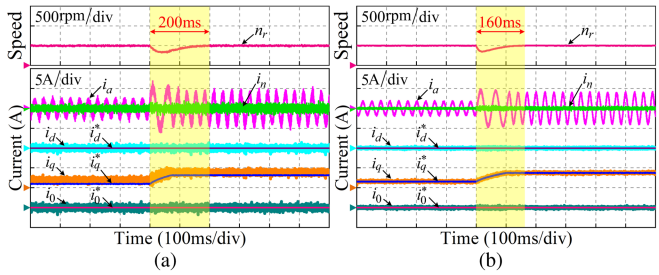

Fig. 33. Experimental data of the two methods in healthy operation mode at 500 r/min with load torque from 2 to 5 N·m under simultaneous multiparameter mismatches ($\Delta R_s = 9R_s$, $\Delta L_{dq} = L_{dq}$, $\Delta L_0 = L_0$, and $\Delta\psi_{\rm f} = \psi_{\rm f}$). (a) DPCC. (b) IDPCC + SMDO.

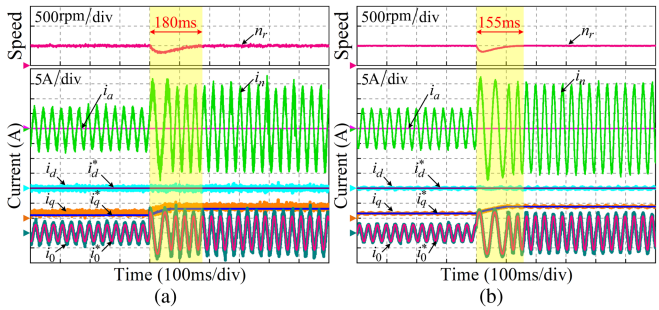

Fig. 34. Experimental data of the two methods in open-phase fault-tolerant operation mode at 500 r/min with load torque from 2 to 5 N·m under simultaneous multiparameter mismatches ($\Delta R_s = 9R_s$, $\Delta L_{dq} = L_{dq}$, $\Delta L_0 = L_0$, and $\Delta\psi_{\rm f} = \psi_{\rm f}$). (a) DPCC. (b) IDPCC + SMDO.

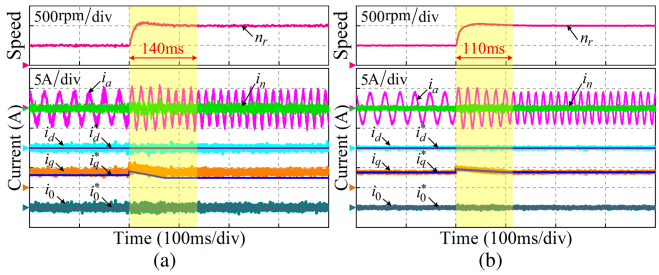

Fig. 35. Experimental data of the two methods in healthy operation mode at 5 N·m with speed from 500 to 1000 r/min under simultaneous multi-parameter mismatches ($\Delta R_s = 9R_s$, $\Delta L_{dq} = L_{dq}$, $\Delta L_0 = L_0$, and $\Delta\psi_{\rm f} = \psi_{\rm f}$). (a) DPCC. (b) IDPCC + SMDO.

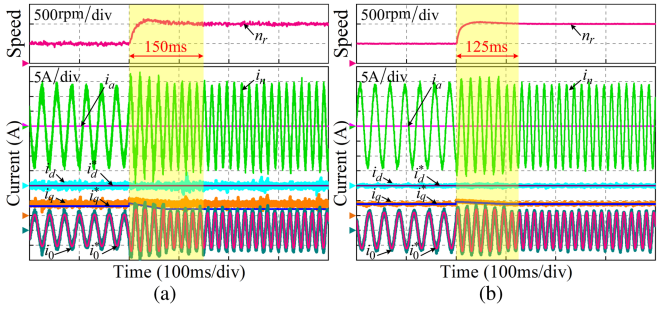

Fig. 36. Experimental data of the two methods in open-phase fault-tolerant operation mode at 5 N·m with speed from 500 to 1000 r/min under simultaneous multi-parameter mismatches ($\Delta R_s = 9R_s$, $\Delta L_{dq} = L_{dq}$, $\Delta L_0 = L_0$, and $\Delta\psi_{\rm f} = \psi_{\rm f}$). (a) DPCC. (b) IDPCC + SMDO.

and its reference. The control performance degradation is even more pronounced in open-phase fault-tolerant operation mode. As depicted in Figs. 28(b) and 32(b), the N-phase current THD for the FCS-MPCC method increases from 17.13% at 1000 r/min to 29.77% at 500 r/min. The d-axis current ripple rises from 2.46 to 5.15 A, while the q-axis current ripple increases from 2.81 to 7.19 A. Although the FCS-MPCC method does not introduce a phase difference in the zero-axis current as observed in the PID case, its zero-axis current ripple also increases significantly in open-phase fault-tolerant operation mode under multiparameter mismatches. In comparison, the proposed IDPCC + SMDO method effectively suppresses the increase in phase current THD and $dq0$-axis current ripple induced by parameter mismatches, while also eliminating the static error in the q-axis current.

B. Dynamic Performance Comparison

In order to evaluate the dynamic performance of the proposed IDPCC + SMDO method, dynamic response comparisons between the DPCC and IDPCC + SMDO methods are conducted based on sudden changes in load torque and target speed, respectively.

At the target speed of 500 r/min and an increment in load torque from 2 to 5 N·m, the experimental outcomes are depicted in Figs. 33 and 34. Clearly, due to multiparameter mismatches, the response time of the DPCC method is longer than that of the proposed IDPCC + SMDO method, even with the same speed loop PI controller. In both healthy and open-phase fault-tolerant operation modes, the tested PMSM drive system using the DPCC method takes 200 and 180 ms, respectively, to recover to the target speed, with a significant speed drop. In contrast, the speed of IDPCC + SMDO method recovers in 160 and 155 ms under the same conditions. Whether in healthy or fault-tolerant operation mode, the $dq0$-axis current ripple and static error of q-axis current caused by multiparameter mismatches lead to large speed fluctuations in the DPCC method, resulting in a slow torque response and preventing the actual speed from quickly tracking the target speed. However, the proposed IDPCC + SMDO method effectively compensates for the current prediction errors caused by multiparameter mismatches, thereby demonstrating better variable load performance compared to the DPCC method.

Figs. 35 and 36 present a dynamic speed response comparison between the two methods under simultaneous multiparameter mismatches, with the load torque held constant at 5 N·m and a sudden increment in target speed from 500 to 1000 r/min. The results indicate that for the conventional DPCC method, the phase current THD and $dq0$-axis current ripple rise as the speed increases, leading to larger speed fluctuations compared to the IDPCC + SMDO method. In addition, the static error of q-axis current also exhibits a growing trend with higher speed. These problems result in the response time of the DPCC method being longer than that of the proposed IDPCC + SMDO method when the target speed suddenly changes. In both healthy and open-phase fault-tolerant operation modes, the tested PMSM drive system using the DPCC method takes 140 and 150 ms, respectively, to reach the target speed, with speed overshoots of 88.6 and 122.4 r/min. In contrast, the speed response time

TABLE II
EXECUTION TIME COMPARISON OF VARIOUS CONTROL METHODS

Method	PID	FCS-MPCC	DPCC	IDPCC + SMDO
Execution time (μs)	18.28	17.96	17.78	20.48

for the IDPCC + SMDO method is 160 and 155 ms under the same conditions, with speed overshoots of 49.5 and 50.7 r/min. Moreover, the proposed IDPCC + SMDO method is unaffected by parameter mismatches and accurately tracks the reference currents in both healthy and fault-tolerant operation modes, with smooth variations in speed and current, as demonstrated in Figs. 35(b) and 36(b).

Based on the above dynamic performance evaluation, the results demonstrate that the proposed IDPCC + SMDO method effectively mitigates the dynamic performance degradation caused by parameter mismatches in DPCC method by enhancing parameter robustness, thereby ensuring satisfactory steady-state and dynamic performance in both healthy and open-phase fault-tolerant operation modes. The execution times of the PID, FCS-MPCC, DPCC, and the proposed IDPCC + SMDO algorithms obtained from the experimental setup are listed in Table II. Although the proposed method introduces a slightly higher computational burden, it remains well within the acceptable range for real-time implementation and does not require any additional hardware.

VI. CONCLUSION

The purpose of this article is to propose an IDPCC + SMDO method to reduce the effects of parameter mismatches on the control performance of PMSM drive systems using four-leg inverters. The major advantages of the proposed method are as follows. 1) An incremental prediction model is established for current prediction in PMSMs with a connected neutral point, effectively eliminating the adverse effects of permanent magnet flux linkage mismatch on the prediction results. 2) A sliding mode observer is designed to compensate for disturbances and uncertainties caused by parameter mismatches, thereby mitigating the impact of resistance and inductance mismatches. 3) The proposed IDPCC + SMDO method can improve the current control performance of the three-phase PMSM drive systems using four-leg inverters by applying predictive current control and compensating for parameter mismatches in the prediction model.

The control performance of the proposed method is verified through comprehensive simulations and experiments conducted on a surface-mounted PMSM. The results demonstrate that the proposed IDPCC + SMDO method achieves satisfactory steady-state and dynamic performance in both healthy and open-phase fault-tolerant operation modes by effectively suppressing the impact of parameter mismatches.

REFERENCES

[1] B. Gan, B. Zhang, and G. Feng, "Design and analysis of modular PM fault tolerant motor for ship direct drive propulsion," *IEEJ Trans. Electr. Electron. Eng.*, vol. 16, no. 9, pp. 1260–1278, Jul. 2021.

[2] Y. Du, T. Tao, and X. Zhao, "Inverter reconstruction approach for open-end winding five-phase PMSM with pattern-based vector synthesis and hybrid SVPWM modulation," *IEEE Trans. Power Electron.*, vol. 39, no. 10, pp. 13597–13612, Oct. 2024.

[3] K. Yu, Z. Wang, and M. Gu, "Universal control scheme of dual three-phase PMSM drives with single open-phase fault," *IEEE Trans. Power Electron.*, vol. 37, no. 12, pp. 14034–14039, Dec. 2022.

[4] P. Xiang, L. Yan, and X. Liu, "Structural topology design for electromagnetic performance enhancement of permanent-magnet machines," *Chin. J. Mech. Eng.*, vol. 38, no. 26, pp. 1–22, Mar. 2025.

[5] A. Gandhi, T. Corrigan, and L. Parsa, "Recent advances in modeling and online detection of stator interturn faults in electrical motors," *IEEE Trans. Ind. Electron.*, vol. 58, no. 5, pp. 1564–1575, May. 2011.

[6] H. Tang, W. Li, and J. Li, "Calculation and analysis of the electromagnetic and temperature field of the PMSM based on fault-tolerant control of four-leg inverters," *IEEE Trans. Energy Convers.*, vol. 35, no. 4, pp. 2141–2151, Dec. 2020.

[7] J. Zhang, W. Zhan, and M. Ehsani, "Fault-tolerant control of PMSM with inter-turn short-circuit fault," *IEEE Trans. Energy Convers.*, vol. 34, no. 4, pp. 2267–2275, Dec. 2019.

[8] A. K. M. Arafat and S. Choi, "Optimal phase advance under fault tolerant control of a five-phase PM assisted synchronous reluctance motor," *IEEE Trans. Ind. Electron.*, vol. 65, no. 4, pp. 2915–2924, Apr. 2018.

[9] X. Wang, Z. Wang, and M. He, "Fault-tolerant control of dual three-phase PMSM drives with minimized copper loss," *IEEE Trans. Power Electron.*, vol. 36, no. 11, pp. 12938–12953, Nov. 2021.

[10] B. Wang, J. Wang, and A. Griffo, "Experimental assessments of a triple redundant fault-tolerant PMASRM drive," *IEEE Trans. Ind. Electron.*, vol. 66, no. 1, pp. 772–783, Jan. 2019.

[11] X. Zhou, J. Sun, and H. Li, "PMSM open-phase fault-tolerant control based on four-leg inverter," *IEEE Trans. Power Electron.*, vol. 35, no. 3, pp. 2799–2808, Mar. 2020.

[12] H. Ghanayem, M. Alathamneh, and R. Nelms, "Performance of a vector controlled PMSM drive based on PR control under single-phase open circuit fault," *Energy Rep.*, vol. 9, pp. 755–763, Mar. 2023.

[13] W. Wang, J. Zhang, and M. Cheng, "Common model predictive control for PMSM drives considering single-phase open-circuit fault," *IEEE Trans. Power Electron.*, vol. 32, no. 7, pp. 5862–5872, Jul. 2017.

[14] D. Xiao, K. S. Alam, and M. P. Akter, "Modulated model predictive control for four-leg inverters with online duty ratio optimization," *IEEE Trans. Ind. Appl.*, vol. 56, no. 3, pp. 3114–3124, Jun. 2020.

[15] J. Rodriguez, C. Garcia, and A. Mora, "Latest advances of model predictive control in electrical drives–Part II: Applications and benchmarking with classical control methods," *IEEE Trans. Power Electron.*, vol. 37, no. 5, pp. 5047–5061, May. 2022.

[16] G. Cimini, D. Bernardini, and S. Levijoki, "Embedded MPC with certified real-time optimization for synchronous motors," *IEEE Trans. Control Syst. Technol.*, vol. 29, no. 2, pp. 893–900, Mar. 2021.

[17] K. Liu, Z. Q. Zhu, and D. A. Stone, "Parameter estimation for condition monitoring of PMSM stator winding and rotor permanent magnets," *IEEE Trans. Ind. Electron.*, vol. 60, no. 12, pp. 5902–5913, Dec. 2013.

[18] K. D. Lee, H.-W. Lee, and J. Lee, "Analysis of motor performance according to the inductance design of IPMSM," *IEEE Trans. Magn.*, vol. 51, no. 3, pp. 1–4, Mar. 2015.

[19] C. Lian, F. Xiao, and J. Liu, "Parameter and VSI nonlinearity hybrid estimation for PMSM drives based on recursive least square," *IEEE Trans. Transport. Electrific.*, vol. 9, no. 2, pp. 2195–2206, Jun. 2023.

[20] S. Nalakath, M. Preindl, and A. Emadi, "Online multi-parameter estimation of interior permanent magnet motor drives with finite control set model predictive control," *IET Electric. Power Appl.*, vol. 11, no. 5, pp. 944–951, 2017.

[21] S. A. Davari, F. Wang, and R. M. Kennel, "Robust deadbeat control of an induction motor by stable MRAS speed and stator estimation," *IEEE Trans. Ind. Informat.*, vol. 14, no. 1, pp. 200–209, Jan. 2018.

[22] Y. Shi, K. Sun, and L. Huang, "Online identification of permanent magnet flux based on extended Kalman filter for IPMSM drive with position sensorless control," *IEEE Trans. Ind. Electron.*, vol. 59, no. 11, pp. 4169–4178, Nov. 2012.

[23] N. Yang, S. Zhang, and X. Li, "A new model-free deadbeat predictive current control for PMSM using parameter-free Luenberger disturbance observer," *IEEE J. Emerg. Sel. Topics Power Electron.*, vol. 11, no. 1, pp. 407–417, Feb. 2023.

[24] Z. Q. Zhu, D. Liang, and K. Liu, "Online parameter estimation for permanent magnet synchronous machines: An overview," *IEEE Access*, vol. 9, pp. 59059–59084, 2021.

[25] L. He, F. Wang, and J. Wang, "Zynq implemented Luenberger disturbance observer based predictive control scheme for PMSM drives," *IEEE Trans. Power Electron.*, vol. 35, no. 2, pp. 1770–1778, Feb. 2020.
[26] X. Li, S. Zhang, and C. Zhang, "An improved DPCC scheme for open-winding PMSMs drives with disturbance observer," *IEEE Trans. Power Electron.*, vol. 36, no. 4, pp. 4622–4632, Apr. 2021.
[27] F. Wang, D. Ke, and X. Yu, "Enhanced predictive model based deadbeat control for PMSM drives using exponential extended state observer," *IEEE Trans. Ind. Electron.*, vol. 69, no. 3, pp. 2357–2369, Mar. 2022.
[28] X. Zhang, B. Hou, and Y. Mei, "DPCC of permanent-magnet synchronous motors with stator current and disturbance observer," *IEEE Trans. Power Electron.*, vol. 32, no. 5, pp. 3818–3834, May. 2017.
[29] Y. Jiang, W. Xu, and C. Mu, "Improved deadbeat predictive current control combined sliding mode strategy for PMSM drive system," *IEEE Trans. Veh. Technol.*, vol. 67, no. 1, pp. 251–263, Jan. 2018.
[30] X. Sun, J. Cao, and G. Lei, "A robust deadbeat predictive controller with delay compensation based on composite SMO for PMSMs," *IEEE Trans. Power Electron.*, vol. 36, no. 9, pp. 10742–10752, Sep. 2021.
[31] R. Zhang, D. Boroyevich, and V. Prasad, "A three-phase inverter with a neutral leg with space vector modulation," in *Proc. Appl. Power Electron. Conf.*, 1997, pp. 857–863.
[32] M. Perales, M. Prats, and R. Portillo, "Three-dimensional space vector modulation in ABC coordinates for four-leg voltage source converters," *IEEE Power Electron. Lett.*, vol. 1, no. 4, pp. 104–109, Dec. 2003.
[33] P. Cortes, J. Rodriguez, and C. Silva, "Delay compensation in model predictive current control of a three-phase inverter," *IEEE Trans. Ind. Electron.*, vol. 59, no. 2, pp. 1323–1325, Feb. 2012.
[34] J. C. Moreno, J. M. Espi Huerta, and R. G. Gil, "A robust predictive current control for three-phase grid-connected inverters," *IEEE Trans. Ind. Electron.*, vol. 56, no. 6, pp. 1993–2004, Jun. 2009.
[35] W. Gao and J. C. Hung, "Variable structure control of nonlinear systems: A new approach," *IEEE Trans. Ind. Electron.*, vol. 40, no. 1, pp. 45–55, Feb. 1993.
[36] S. Kwak, S.-E. Kim, and J.-C. Park, "Predictive current control methods with reduced current errors and ripples for single-phase voltage source inverters," *IEEE Trans. Ind. Informat.*, vol. 11, no. 5, pp. 1006–1016, Oct. 2015.

Yuchen Zhou received the B.S. degree in mechatronics from the Chongqing University of Science and Technology, Chongqing, China, in 2018, and the M.S. degree in mechanical design and theory from the Nanjing University of Aeronautics and Astronautics, Nanjing, China, in 2021. He is currently working toward the Ph.D. degree in mechatronics from Beihang University, Beijing, China.

His research interests include the design and control of permanent magnet machines.

Liang Yan (Senior Member, IEEE) received the B.S. degree in mechatronics from the North China Institute of Technology, Taiyuan, China, in 1995, the M.S. degree from the Beijing Institute of Technology, Beijing, China, in 1998, and the Ph.D. degree in mechatronics in mechatronics from Nanyang Technology University, Singapore, in 2006.

He is currently a Professor with Beihang University, Beijing. His research interests include robotics, actuators, and mechatronic systems.

Dr. Yan is a Member of Electrical Machines Technical Committee of the IEEE Industrial Electronics Society.

Xiaocheng Wei received the B.S. degree in electric and electronic engineering and M.S. degree in control science and engineering from the North University of China, Taiyuan, China, in 2014 and 2017, respectively. He received the Ph.D. degree in electric machines from the University of Nottingham, Nottingham, U.K., in 2022.

He is currently an Associate Professor with the Ningbo Institute of Technology, Beihang University, Ningbo, China. His research interests include high-performance motor, hybrid electric propulsion system, and PM generator.

Mostafa S. Hamad (Senior Member, IEEE) received the B.Sc. and M.Sc. degrees in electrical engineering from Alexandria University, Alexandria, Egypt, in 1999 and 2003, respectively, and the Ph.D. degree in electrical engineering from Strathclyde University, Glasgow, U.K., in 2009.

He is currently a Professor with the Department of Electrical and Control Engineering, College of Engineering and Technology, Arab Academy for Science, Technology and Maritime Transport, Alexandria. His research interests include power electronics applications in power quality, electric drives, distributed generation, HVDC transmission, and renewable energy.